

Flexible Tactile Sensing Microfibers Based On Liquid Metals

Shuting Liang,* Jie Li, Fengjiao Li, Liang Hu, Wei Chen, and Chao Yang

Cite This: *ACS Omega* 2022, 7, 12891–12899

Read Online

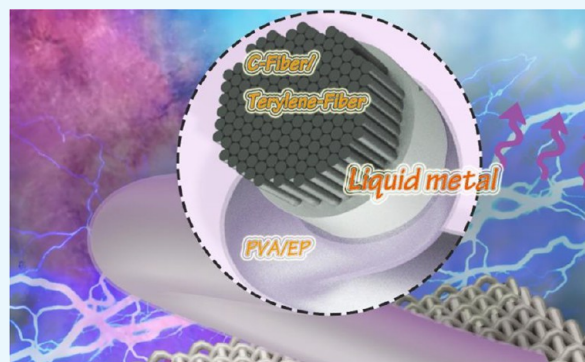
ACCESS |

Metrics & More

Article Recommendations

Supporting Information

ABSTRACT: High-performance and intelligent fibers are indispensable parts of wearable electronics in the future. This work mainly demonstrates the preparation of flexible intelligent liquid metal (LM) fibers with three core–sheath structures. An ultra-thin (10–50 μm), conductive, and highly flexible LM was deposited on the fiber core [carbon/polyethylene terephthalate (C/PET)—150–500 μm] along the fiber direction and then deposited on a polymer-protective layer [polyvinyl alcohol/epoxy resin (PVA/EP)—10 μm]. Four kinds of LM intelligent fibers were manufactured, including the C–LM–PVA fiber, C–LM–EP fiber, PET–LM–PVA fiber, and PET–LM–EP fiber. These LM intelligent fibers (diameter, 150–600 μm) were demonstrated with a high conductivity of $7.839 \times 10^4 \text{ S}\cdot\text{m}^{-1}$. The changes in resistance in different torsion directions were measured, and these smart LM fibers could also be used as electrical heaters or thermoelectric generators, which released heat (36–36.9 $^\circ\text{C}/1\text{--}1.5 \text{ V}$) into the environment. Then, these multifunctional LM fibers were applied as high-performance strain sensors and bending sensors. These flexible LM conductive fibers could be successfully utilized in intelligent wearable fabrics and were expected to be widely utilized in artificial muscle and sensor fields.



INTRODUCTION

Intelligent composite materials could change their performance parameters and mimic life systems in real time and adapt to the changing environment. The application of conductive fibers is very wide, including in electric storage medium, power generation medium, sensing medium, heating medium, energy collection, and information sensing.¹ The traditional fibers have a variety of excellent properties; nevertheless, they lack electrical conductivity and intelligence. Recently, the fibers and fiber assembly with a function of sensing information have been attracting significant interest in a wide range of fields, especially in clothing with smart fibers, which have the ability to respond and feedback information.²

Intelligent fibers with sensing functions to external stimuli, such as stress, strain, light, electricity, magnetism, and biochemistry, could be utilized to make various sensors.³ As a part of intelligent textiles, they could not only perceive the external environment or internal state changes and stimulation but also make a response.⁴

Nowadays, smart fabrics could automatically adjust the temperature according to the environment.⁵ For example, multiwalled carbon nanotubes and polypyrrole are deposited on the surface of cotton fibers as a framework to construct functional fibers with excellent electrochemical, electrothermal, and bactericidal properties.⁶ Subsequently, silver nanowires are utilized to deposit on carbon nanotubes to prepare composite fiber materials with excellent electrical conductivity and elasticity.⁷ In addition, styrene–ethylene–butylene–styrene

rubber could also be utilized as a nucleus, wrapped with carbon nanotubes to form superelastic conductive fibers, and be applied in tension sensors and electric artificial muscles.⁸ By impregnating nylon fibers with liquid crystal (CLC) and polymer (PVP) solutions, liquid crystal fibers with different responses and wearable sensors could be obtained.⁹ Furthermore, by deposition of tungsten trioxide (WO_3) and poly(3-methylthiophene) on the fiber electrode, electrochromic fibers could be prepared.¹⁰

The commonly used conductive metal materials of the traditional flexible fiber are stainless steel, copper, silver, and nickel. In addition, the commonly used fiber wrapping materials mainly include graphene, carbon nanotubes,⁵ silver nanowires,⁶ and shape-memory materials. However, solid metals are hard and fail easily under strain, which are not conducive to the preparation of flexible fibers. Another conventional method is to bury the metal wire in the fabric, which is suitable only for the highly rigid and small deformation products. In particular, this fabric does not have good stitchability and wearing comfort, which limit its application.

Received: January 10, 2022

Accepted: March 21, 2022

Published: April 4, 2022



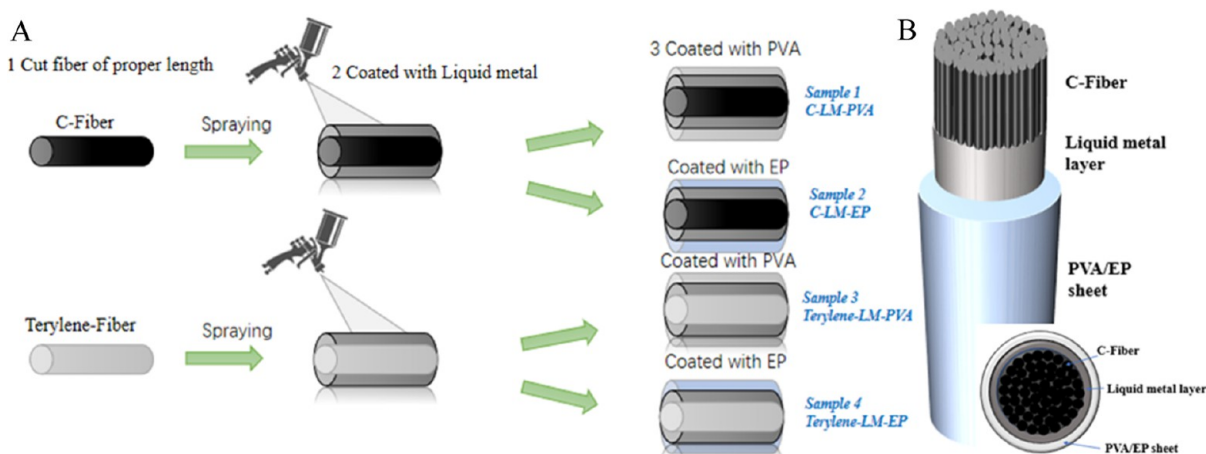


Figure 1. (A) Flowchart of the preparation and production process of a LM flexible fiber. (B) Illustration of the structure of the LM smart fiber.

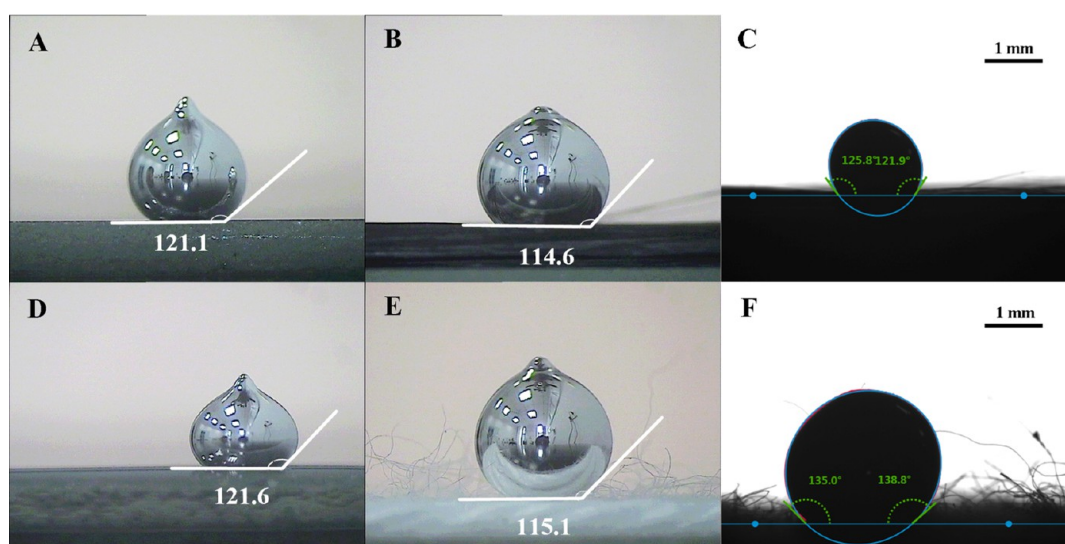


Figure 2. Contact angle testing of LMs: (A) contact angle measurement between LM and PVA; (B,C) contact angle measurement between LM and carbon fiber and its black and white diagram; (D) contact angle measurement between LM and epoxy resin; and (E,F) contact angle measurement between LM and polyester and its black and white picture.

To overcome these limitations, there are several emerging strategies for creating flexible fibers, and liquid metals (LMs) may represent one of the candidate materials.¹¹ Owing to their excellent electrical conductivity, thermal conductivity, and low toxicity, they have been receiving considerable attention to tackle current challenges.^{12–21} To the best of our knowledge, the research of LM composite fibers is in the initial stage.^{12,22–26} Furthermore, there has been a steady growth of research papers in this field,^{27–30} reporting various LM composite fiber sensors, including self-powered sensors,³¹ implantable biosensors,³² selective biosensors,³³ strain sensors,³⁴ and capacitive sensors.³⁵ For example, Wu previously reported the LM microfibers as self-powered sensors.³⁶ It has been reported that LM fibers could harvest energy from triboelectricity as well.³¹

In this report, we aim to develop a LM fiber that has multifunctions of pressure sensing, bending sensing, and thermoelectric generation. We spray the carbon or polyethylene terephthalate (PET) microfibers with a eutectic gallium–indium alloy. The LM smart fiber is constructed from the carbon fiber/PET fiber, LM, and polyvinyl alcohol [PVA, (C₂H₄O)_n]/epoxy resin [EP, (C₁₁H₁₂O₃)_n] material. In particular, the obtained C–LM–EP, C–LM–PVA, terylene–

LM–EP, and terylene–LM–PVA fibers show excellent electrical performance. We demonstrate that this LM smart fiber can generate thermal radiation from electricity and has an electrothermal property. Finally, this LM smart fiber could be utilized as a bending sensor, touch sensor, and gesture sensor.

RESULTS AND DISCUSSION

Four different smart LM fibers were fabricated, which include the (1) C–LM–EP fiber; (2) C–LM–PVA fiber; (3) terylene–LM–EP fiber; and (4) terylene–LM–PVA fiber.

Figure 1B(b) shows the structure of the prepared LM smart fiber. This fiber was divided into three layers: the inner core of this fiber was carbon or a polyester material. The middle layer of this fiber was the LM material. The outer layer of this fiber was an epoxy resin or PVC wrapping materials.

As illustrated in Figure 1A, the manufacturing process of the LM flexible intelligent fiber was divided into three representative strategies:

- (i) Carbon fiber (3k) or polyester materials were selected to prepare the inner core of the flexible fiber. First, an ideal length (20 cm) of carbon fiber or polyester fiber was cut

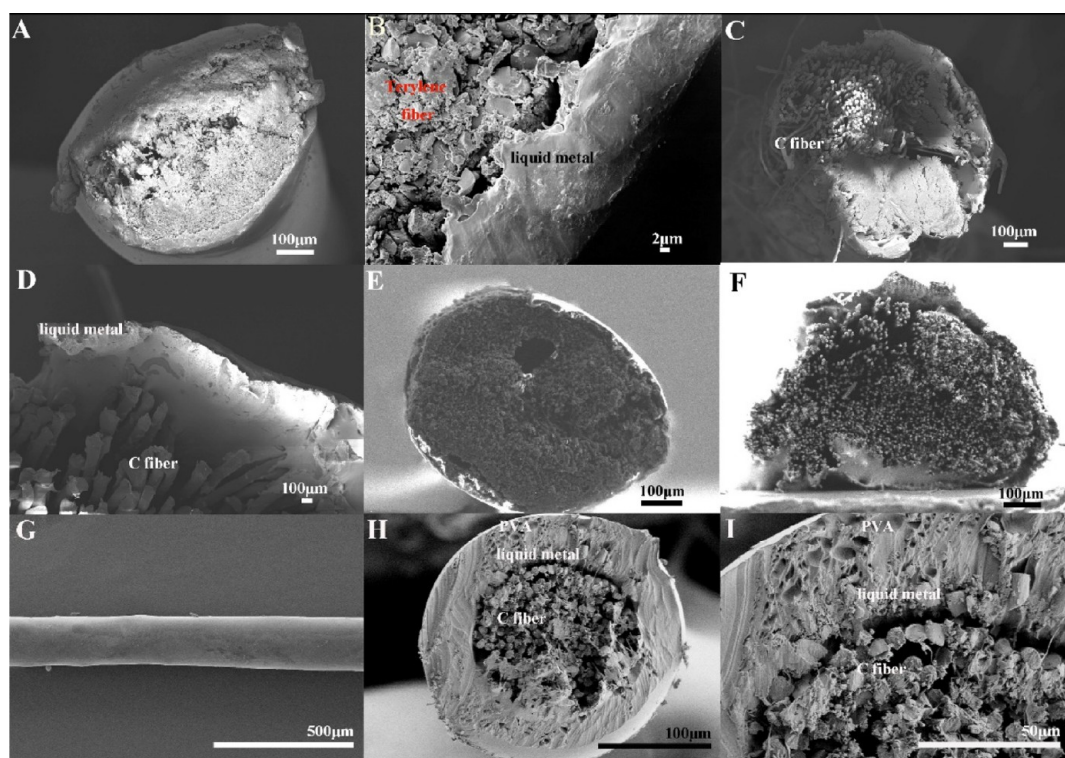


Figure 3. SEM image of LM flexible fibers: (A,B) SEM image of the LM flexible fiber made of polyester: terylene–LM; (C) SEM images of flexible C–LM–PVA fibers; (D) local enlarged SEM image of a C–LM–PVA fiber; in the middle is a single C filament; (E) SEM images of a flexible C–LM–PVA fiber; (F) SEM images of a flexible C–LM–EP fiber; (G–I) superfine C–LM–PVA fiber: (G) SEM image of the side view of a superfine C–LM–PVA fiber; (H) SEM image of a superfine C–LM–PVA fiber; and (I) local enlarged SEM image of a superfine C–LM–PVA fiber.

and placed on a fixed suspension platform. The conductivity of the carbon fiber was good, while the polyester fiber had insulating properties. Thus, the different prepared fibers could have different conductive properties.

- (ii) Second, the ends of these removed fibers were fixed and horizontally hung. LM was packed into the container of a spray pen and evenly sprayed into this carbon fiber or polyester fiber. Correspondingly, the finished LM-coated fiber was removed from the device, and this fiber would be vertically suspended for about 0.5–1 h. Then, the LM fully contacted and adhered to the inner fiber.
- (iii) The third step was to encapsulate the suspended fibers. PVA and EP were selected as packaging materials. The packaged adhesive was evenly sprayed on the hanging LM fiber to achieve the purpose of packaging and protection. The encapsulated fibers coated with packaging materials were vertically suspended for about 24 h. The purpose of the suspension was to allow excess packaging materials to drip off and make the fibers better shaped into a solid state. Then, the LM flexible fiber was successfully prepared.

In order to test the adhesion behavior of LMs with carbon, polyester, PVA, and epoxy resin materials, the contact angles of LM droplets on these four materials were measured at room temperature. As illustrated in Figure 2A–F, the LM was dropped onto solid surfaces which were covered with PVA, carbon fiber, epoxy resin, and polyester fiber material to test the contact angles between the LM and these materials, respectively.

As illustrated in Figure 2, the experimental result shows that the contact angles between the LM and PVA, carbon fiber, epoxy

resin, and polyester materials were about 121.1, 114.6, 121.6, and 115°, respectively. The contact angle between the LM and PVA was smaller than the contact angle between the LM and epoxy resin. Thus, the adhesion force of the LM to PVA was greater than that of the LM to epoxy resin. The contact angle between the LM and carbon fiber was smaller than the contact angle between the LM and polyester. Thus, the adhesion force of the LM to carbon fiber was greater than that of the LM to polyester fiber. The compactness of the composite fiber in the wrapping process would be affected by adhesion behaviors. If the LMs have excellent adhesion behaviors with other materials, which may cause the LM to bind more tightly to materials, then the fibers would be more compact. LMs could easily peel off from the material that does not adhere well. As a result, the fiber is not tight, which affects the electrical conductivity and sensitivity.

In addition, to observe whether the LM flexible fibers have a structure of core–middle–cortex layer, scanning electron microscopy (SEM) and energy-dispersive X-ray spectroscopy (EDXS) of flexible fibers were performed as well.

Figure 3A,B shows the overall SEM image of the LM flexible fiber made of polyester, while Figure 3B is the enlarged cross-sectional image. It could be seen that the diameter of the prepared LM smart fiber was 638 μm, and the total thickness of the middle layer and outer layer was 25–65 μm. It was not difficult to find that the produced smart fiber presented an annual ring-like structure. The core layer was fiber, the middle layer was the LM, and the skin layer was the encapsulation material. The surface of the flexible LM fiber was smooth, and the wrapping of the material was complete.

Figure 3C–F shows the overall SEM image of the LM flexible fiber made of carbon fibers, including C–LM–PVA fiber

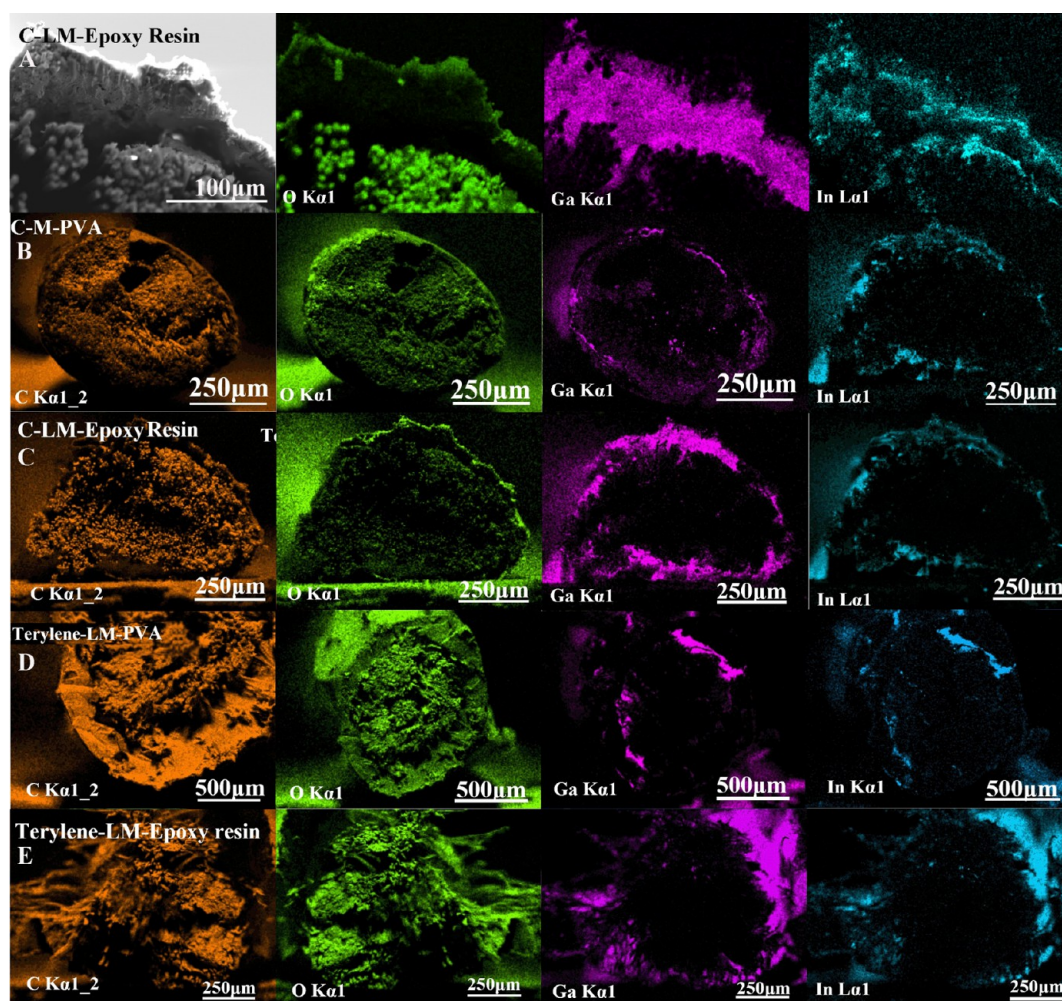


Figure 4. (A) Thickness of the middle layer and the cortex of the LM fiber; SEM (Scanning Electron Microscopy) and EDS (Energy Dispersive Spectrometer) diagrams of four fibers: (B) EDS test diagrams of the C-LM-PVA fiber; (C) EDS test diagrams of the C-LM-EP fiber; (D) EDS test diagrams of the terylene-LM-PVA fiber; and (E) EDS test diagrams of the terylene-LM-EP fiber.

(Figure 3C,E) and C-LM-EP fiber (3F), while Figure 3D shows the enlarged SEM cross-sectional image. The diameters of the prepared C-LM-PVA fiber and C-LM-EP fiber were 552 and 576.4 μm , respectively. Owing to the 3k carbon fiber, it could be seen from the SEM image that there were 3000 carbon fibers inside the smart fiber, and the outside was wrapped with a micrometer-level LM layer. Figure 3E,F shows the profiles of C-LM-PVA and C-LM-EP fibers, respectively. It could also be seen that the packaging effect of PVA was better than that of the epoxy resin.

By reducing the number of carbon precursors in the carbon fiber, the diameter of the carbon fiber could be reduced. Then, the prepared LM fiber could be finer. Figure 3G–H illustrates that this LM fiber (diameter of 200 μm) has a uniform and regular surface. The width of the PVA layer was 7 μm , the width of the LM layer was 23 μm , and the diameter of this C fiber was only 128 μm (in Figure 3H).

Figure 4A shows the thickness of the middle layer and the cortex of the fiber. As the packaging materials contained an O element (green figure), the thickness of the packaging layer could be judged according to the O element. The LM materials contained Ga and In elements (purple and blue figures), and the thickness of the LM layer could be judged according to the Ga element. The thickness of the outermost layer of the C-LM-EP

fiber was 19 μm , and the thickness of the middle LM layer was 45.5 μm .

Figure 4B–E shows the EDS test diagrams of the C-LM-PVA fiber, C-LM-EP fiber, terylene-LM-PVA fiber, and terylene-LM-EP fiber. The orange and green figures show the elemental distribution of carbon (C) and oxygen (O), respectively. It could be clearly observed from Figure 4B–E that the LM flexible fibers have three layers of structure, namely the core layer, middle layer, and cortex.

From Figure 4, it can be observed that the inner core of the LM flexible fiber was a carbon fiber or a polyester fiber, which was mainly composed of a C element. The central layer of the flexible fiber was a LM, which mainly contained Ga and In elements. The outer layer of the flexible fiber was polymer PVA and EP materials, which mainly contained C, H, and O elements.

The LM flexible fiber has some electrical conductivity. Under different voltages, several LM flexible fibers were connected to the power supply. The current changes of these fibers were tested. Figure 5A shows the voltage–current (V – I) diagram of C-LM-EP and C-LM-PVA fibers. When a certain voltage was applied to these fibers, these fibers have a constant current. When the voltage increased from 0 to 1.4 V, the current of C-LM-PVA and C-LM-EP fibers also increased from 0.05 to 0.35 A. Therefore, from eq 1, the average resistance values (R /

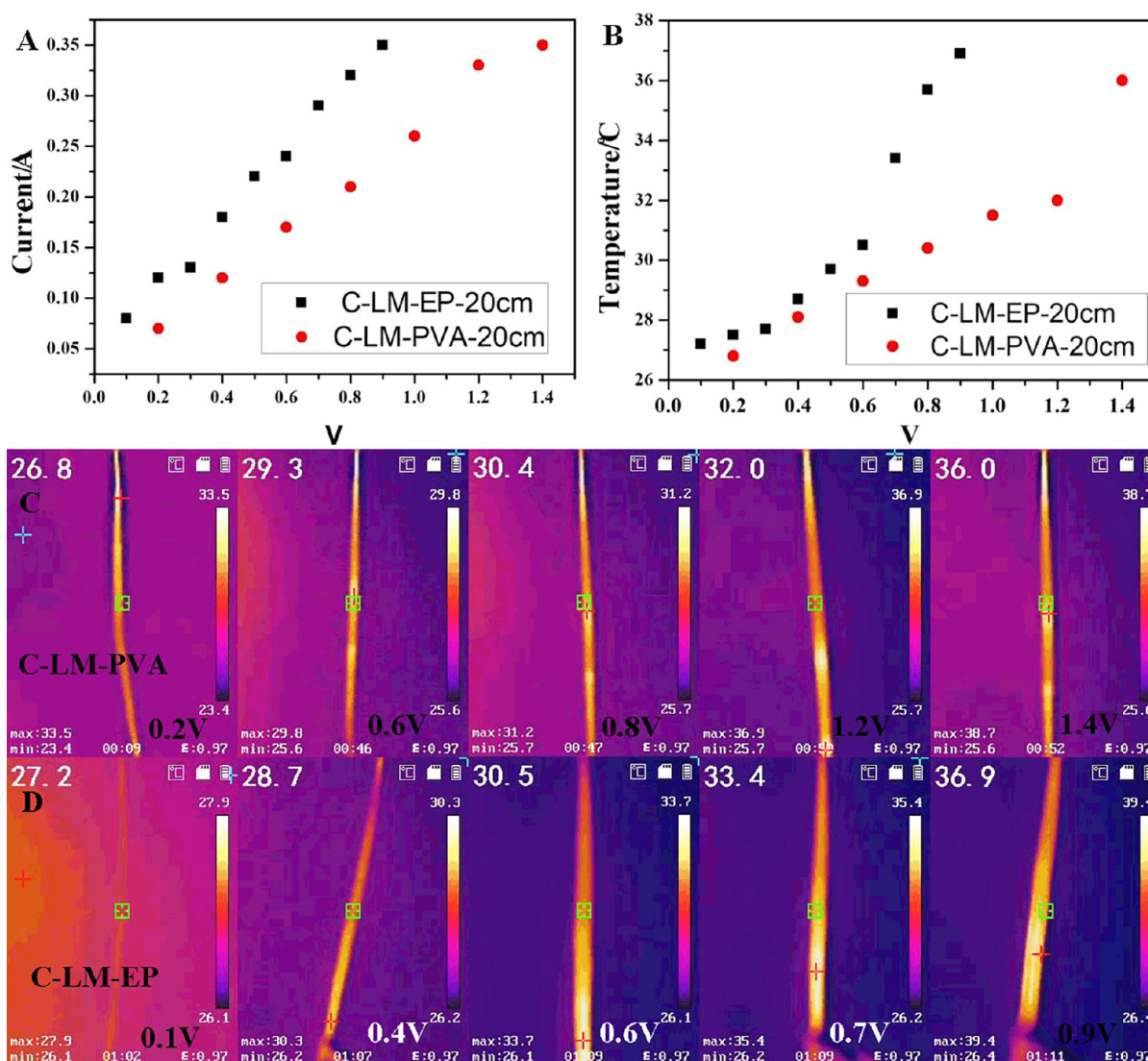


Figure 5. Testing of the electrical property and thermal property of LM fibers: (A) voltage–current relation diagram of the C–LM–EP fiber and C–LM–PVA fiber; (B) voltage–temperature relation diagram of the C–LM–EP fiber and C–LM–PVA fiber; (C) infrared imaging of the C–LM–PVA fiber; and (D) infrared imaging of the C–LM–EP fiber.

Ω) of the C–LM–EP fiber and C–LM–PVA fiber (20 cm length) could be calculated, divided into $R_{C-LM-EP}$ and $R_{C-LM-PVA}$

$$R = \frac{V}{A} \quad (1)$$

The average resistance value ($R_{C-LM-EP}$) of the C–LM–EP fiber (20 cm length) was 2.445 Ω , while the average resistance value ($R_{C-LM-PVA}$) of the C–LM–PVA fiber (20 cm length) was 3.79 Ω . When the packaging layer was different, the resistance value of the LM flexible fiber was different. The LM flexible fiber packed with PVA has a higher resistance value.

From eq 2, the average resistivity values (ρ) of C–LM–EP fiber and C–LM–PVA fiber (20 cm length) could be calculated, divided into $\rho_{C-LM-EP}$, and $\rho_{C-LM-PVA}$

$$R = \frac{\rho * L}{S} \quad (2)$$

For C–LM–EP: $R_{C-LM-EP} = 2.445 \Omega$; $L = 20 \text{ cm} = 0.2 \text{ m}$; and $S = 1.0434 \times 10^{-6} \text{ m}^2$, wherein L is the length of the C–LM–EP fiber and S is the cross-sectional area of the C–LM–EP fiber.

From Figure 3, the diameters of the prepared C–LM–PVA fiber and C–LM–EP fiber were observed to be 552 and 576.4 μm , respectively. Thus, $S = \pi R^2 = 3.14159 * (576.4 \mu\text{m})^2 = 3.14159 * (5.764 \times 10^{-4} \text{ m})^2 = 1.0434 \times 10^{-6} \text{ m}^2$. Thus, $\rho = 1.27566 \times 10^{-5}$, and $\sigma_{C-LM-EP} = 1/\rho = 7.839 \times 10^4 \text{ S} \cdot \text{m}^{-1}$.

For C–LM–PVA: $R_{C-LM-PVA} = 3.79 \Omega$; $L = 20 \text{ cm}$; and $S = 0.95807 \times 10^{-6} \text{ m}^2$. From Figure 3, the diameter of the prepared C–LM–PVA fiber was observed to be 552 μm . Thus, $S = \pi R^2 = 3.14159 * (552 \mu\text{m})^2 = 0.95807 \times 10^{-6} \text{ m}^2$. Thus, $\rho = 1.81554 \times 10^{-5}$ and $\sigma_{C-LM-PVA} = 1/\rho = 5.508 \times 10^4 \text{ S} \cdot \text{m}^{-1}$.

Therefore, the average electrical conductivity ($\sigma_{C-LM-EP} = 1/\rho$) of the C–LM–EP fiber was $7.839 \times 10^4 \text{ S} \cdot \text{m}^{-1}$, while the average electrical conductivity ($\sigma_{C-LM-PVA}$) of the C–LM–PVA fiber was $5.508 \times 10^4 \text{ S} \cdot \text{m}^{-1}$, which were lower than that of pure LM ($3.46 \times 10^6 \text{ S} \cdot \text{m}^{-1}$).³⁰

Figure 5B shows the voltage applied to the LM smart fiber. For each prepared LM smart fiber, when the voltage increased to a certain value, the voltage value has a maximum voltage value (V_{max}). For example, the maximum value of the applied voltage of the C–LM–PVA fiber was 1.4 V ($V_{\text{max}} = 1.4 \text{ V}$).

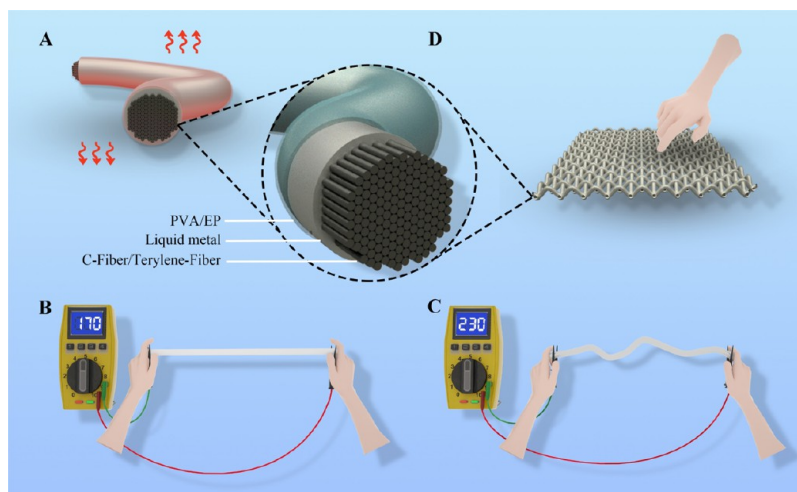


Figure 6. Flexible LM tactile sensing fiber: (A) structure of the LM fiber; (B,C) electrical signal of the intelligent fiber changing with the action of an external force; and (D) smart fibers having the sensing property.

In Figure 5B, the black and red dots denote the voltage–heat (V – T) diagrams of the C–LM–EP fiber and C–LM–PVA fiber, respectively. When a certain voltage was applied to the fiber, the temperature of the fiber gradually raised to a constant value. The experimental results showed that the LM flexible fiber has a certain heat release property. Under a weak voltage, it could provide a certain amount of heat which was suitable for human body temperature.

Figure 5C,D shows the thermal images of two kinds of LM flexible fibers (C–LM–PVA and C–LM–EP fibers). When different voltages were applied to the LM flexible fibers, these smart fibers could release heat to the environment. As could be seen from the thermal image, the orange region was the thermal image of the LM flexible fiber, and the purple region was the external environment with a temperature of 23–25 °C. When the voltage of the C–LM–PVA fiber increased from 0 to 1.4 V, the released heat accordingly increased, and the temperature increased from 26.8 to 36 °C. The maximum voltage of the C–LM–PVA fiber was 1.4 V. When the voltage of the C–LM–EP fiber increased from 0 to 0.9 V, the temperature increased from 27.2 to 36.9 °C. The maximum voltage of the C–LM–EP fiber was 0.9 V. When the packaging layer was different, the exothermic temperature of the LM flexible fiber was different.

As illustrated in Figure 6, in the case of an external power supply, the angle of the intelligent fiber would change with the action of an external force, which would lead to the resistance change of the fiber. This was evident from the Supporting Information Movies S1–S3. As could be seen in the movies and Figure 6B,C, depending on the external force, the resistance of the C–LM–PVA fiber varied from 16.8 to 23.1 Ω , while the resistance of the C–LM–EP fiber varied from 5.8 to 9.8 Ω .

Because of their good flexibility and electrical conductivity, the LM fibers could be made into flexible pressure sensors and bending sensors. The bending sensing performances of the LM flexible fiber were also tested. Figure 7A,B shows the force analysis diagrams of the flexible LM fiber. When external forces such as pressure and bending force were applied to LM fibers, the shape of the inside LM was changed. Because the LM was compressed, the resistance of the smart fiber changed.

By attaching the prepared LM fibers onto a glove, a gesture sensor was built. As shown in Figure 7C,D, LM sensing fibers were attached to each finger. The end of the flexible LM sensing

fiber was connected to a copper wire, and LM intelligent sensing gloves could be prepared. The end of the copper wire was connected to a multimeter (Figure 7D).

The LM composite fibers were detected by tactile signals, including finger bending signals. As shown in Figure 7E,F, by changing the different bending degrees of the finger, the change of the electrical signal of the LM smart fiber was detected.

The prepared LM fiber was also attached to the back of the glove to form a pressure sensor. As shown in Figure 7E,F, the LM fibers on the back of the hand were pressed, and the changes of electrical signals were detected.

As shown in Figure 7G, the abscissa value was the angle, and the ordinate value was the resistance change $((R - R_0)/R_0)$ of the C–LM–PVA fiber. According to the data, the sensitivity of the fiber first increased and then decreased.

As shown in Figure 7H, the abscissa value was the pressure (kPa), and the ordinate value was the resistance change $((R - R_0)/R_0)$ of the C–LM–PVA fiber.

The LM sensor was pressure-tested by a multifunctional testing machine (Supporting Information S4) and a push–pull meter. The resistance of the LM sensor was measured using a digital multimeter. Further, the sensitivity (S) of the LM sensor was tested. The measurement formula of sensitivity (S/kPa^{-1}) is

$$S = \frac{\Delta R}{R_0} P = \frac{R - R_0}{R_0} P \quad (3)$$

where $R - R_0 = \Delta R$ is the change value of resistance when pressure is applied; R_0 is the initial resistance when no pressure is applied; and P is the load pressure. When external pressure stimulation results in a change in the resistance (R) of the sensor, induced by an external mechanical force, the thickness of the LM layer changes and the effective contact area of the LM layer also changes.

For the LM sensor, the abscissa value was the pressure (Pa), and the ordinate value was the resistance change $((R - R_0)/R_0)$ of the fiber. The linearity of the sensor is the degree to which the output–input curve deviates from the fitting straight line.

We also measured the detection limit of this LM pressure sensor fiber, which is the minimum pressure value that can be detected, and its pressure sensing working range (Pa to kPa). The working range of this sensor is 0 Pa to 140 kPa.

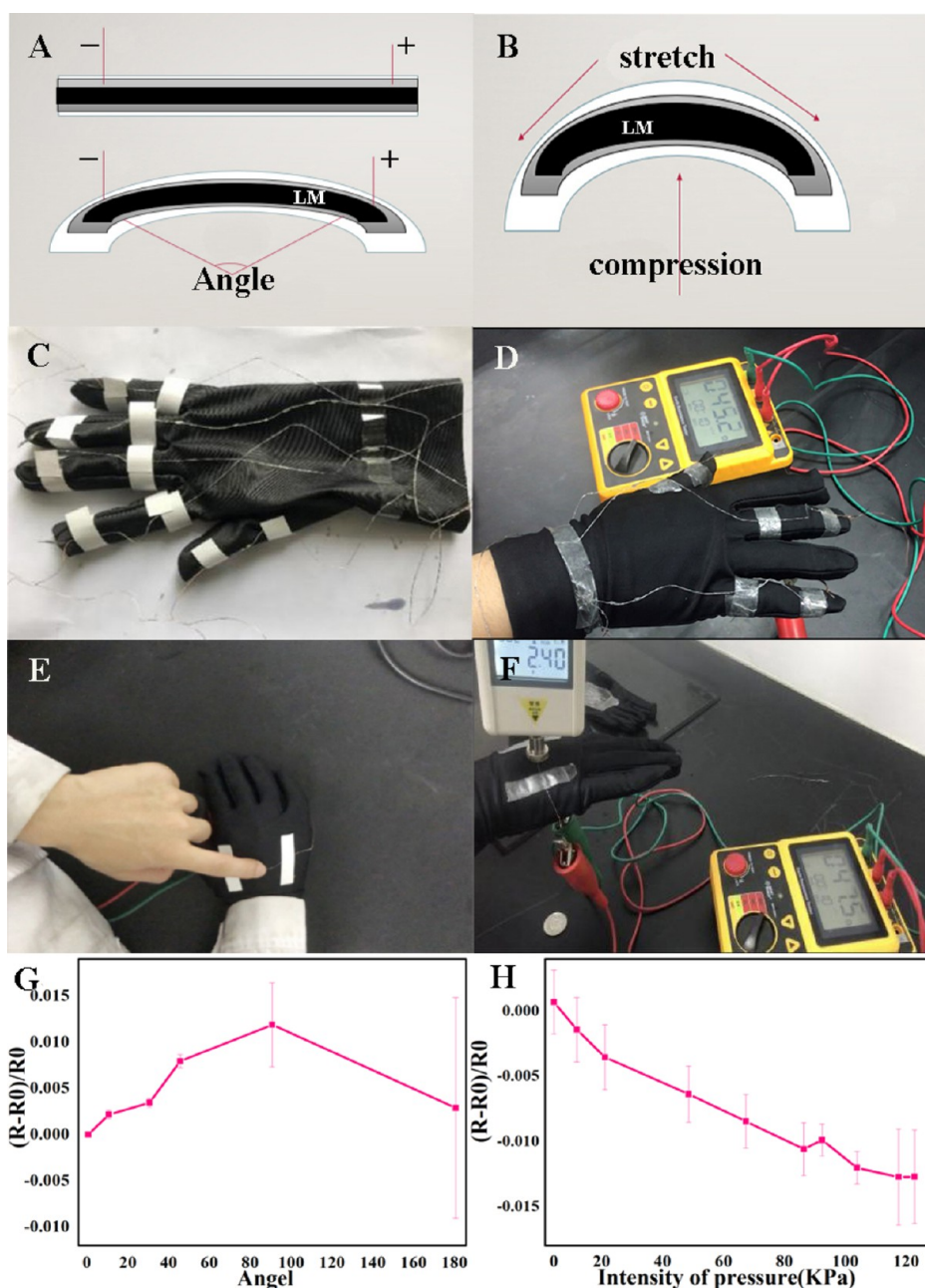


Figure 7. (A,B) Stress analysis diagram of a LM bending sensor; (C) LM fiber sensor; (D) sensitivity test of the LM bending sensor smart glove; (E,F) performance test of the LM fiber sensor; (G) sensitivity change of the LM bending sensor; and (H) sensor sensitivity test data of the LM fiber.

Hence, resolution = $\Delta X_{\min}/X_{FS} \times 100\% = 20 \text{ kPa}/140 \text{ kPa} = 14.28\%$.

CONCLUSIONS

In summary, in this paper, a facile way to spray LMs on common carbon fibers and terylene fibers was demonstrated, which could make the ordinary nonconductive fibers conductive and smart. The LM flexible tactile sensing fiber consisted of a three-layer sheath–core structure, the core layer, the middle layer, and the cortex structure. The fibers coated with PVA have better flexural and flexible properties.

The LM intelligent fibers have shown excellent electrical performance ($7.839 \times 10^4 \text{ S}\cdot\text{m}^{-1}$). One interesting outcome of this work is that when the applied voltage was applied at both ends of the LM flexible tactile sensing fiber, it was found that the

voltage value could not continue to increase ($V_{\max} = 1.4 \text{ V}$) when the voltage increases to a certain value. Further, the highest temperature at which the fiber could rise to a constant value, $T_{\max} = 36.9 \text{ }^\circ\text{C}$.

Finally, this LM smart fiber could be utilized as a bending sensor, touch sensor, gesture sensor, and thermoelectric generator. As the angle of external force changes, the fiber resistance would change, which has potential applications in flexible intelligent fibers.

EXPERIMENTAL SECTION

Materials and Methods. The LM was uniformly mixed with Ga and In, and its mass ratio was 75.5:24.5. Gallium (purity of 99.9%) and indium (purity of 99.9%) were purchased from Shanghai MacLean Metal Materials Co., Ltd.

The preparation method of LM was as follows: the configured Ga and In were placed in a suitable beaker; the beaker was placed in a water bath; the temperature of the water bath was set to 70 °C; and the metals were heated in a water bath. The prepared metals were heated to a molten state and then a magnetic stirrer was added to the beaker to magnetically stir the molten metals below 70 °C for 1 h to obtain a uniformly mixed LM.

The carbon (C) fiber is a kind of conductive fiber, and it was purchased from Dongguan Ulida Co., Ltd., with a purity of 99% and a specification of 3k. The polyester fiber (PET) is a nonconductive fiber, which was purchased from Tianjin Goods Company, with a purity of 99% and a diameter of 1 mm. PVA was purchased from Shanghai Colaoli International Trade Co. Ltd., with a purity of 99%. EP was purchased from Quanzhou Yasson Company, with a purity of 98%. The EP and curing agent were configured according to the mass ratio of 3:1. Further, PVA and distilled water were configured according to the mass ratio of 1:10.

The airbrush was purchased from the VOGUE Company, and it was an HD-470 upper pot airbrush, and the model was NUE LP-130. The handheld thermal camera was purchased from HIKVISION Company, with the model DS-2TPH10-3AUF. The digital multimeter was purchased from VICTOR Company with the model VC9808. The DC voltage supplier was purchased from Chongqing Jin Heng Materials Co., Ltd., with the model UNI-T UTP3305.

Characterization. The shape and diameters of the LM fibers were obtained using a scanning electron microscope (ZEISS, FEI Quanta 250, US, WD working distance: 4.1–5.8 mm, EHT acceleration voltage: 200–30 kV, magnification: 28–440 \times , InLens detector). The energy-dispersive spectrum was obtained with a JEOLJEM 2010 operating at an acceleration voltage of 200 kV.

As shown in Figure S4 (Supporting Information), the LM pressure sensor was placed at the end of the pressure gage. The end of the pressure sensing fiber was connected to the multimeter. The handwheel was slowly rotated to apply downward pressure. The pressure gage was used to accurately read the amount of downward pressure applied. Further, the multimeter was used to record the resistance changes of sensing fibers under different pressures.

■ ASSOCIATED CONTENT

SI Supporting Information

The Supporting Information is available free of charge at <https://pubs.acs.org/doi/10.1021/acsomega.2c00098>.

EDS test diagrams of C–LM–PVA, C–LM–EP, terylene–LM–PVA, and terylene–LM–EP fibers; digital camera photos of the prepared fibers; sensitivity regression line and stress measurement; elasticity and tensile limit test of LM fiber; and electrical resistance of different fibers (PDF)

Resistance of the intelligent fiber would change with the action of an external radial force (MP4)

Resistance of the intelligent fiber changing with the angle (MP4)

Resistance of the intelligent fiber would change with the action of an external axial force (MP4)

Changes in electrical signals of LM pressure sensor fibers (MP4)

■ AUTHOR INFORMATION

Corresponding Author

Shuting Liang – College of Chemical and Environmental Engineering and Chongqing Key Laboratory of Environmental Materials & Remediation Technologies, Chongqing University of Arts and Sciences, Chongqing 402160, PR China; orcid.org/0000-0002-7772-0757; Email: stliang@mail.tsinghua.edu.cn

Authors

Jie Li – College of Chemical and Environmental Engineering, Chongqing University of Arts and Sciences, Chongqing 402160, PR China

Fengjiao Li – Shenzhen Automotive Research Institute, Beijing Institute of Technology, Shenzhen 518118, PR China

Liang Hu – Key Laboratory of Biomechanics and Mechanobiology, Ministry of Education Beijing Advanced Innovation Center for Biomedical Engineering, School of Biological Science and Medical Engineering, Beihang University, Beijing 100083, PR China

Wei Chen – College of Chemical and Environmental Engineering, Chongqing University of Arts and Sciences, Chongqing 402160, PR China

Chao Yang – College of Chemical and Environmental Engineering, Chongqing University of Arts and Sciences, Chongqing 402160, PR China

Complete contact information is available at:

<https://pubs.acs.org/10.1021/acsomega.2c00098>

Author Contributions

S.L. was in charge of the whole trial and wrote the manuscript; J.L. wrote part of the manuscript; and F.L., L.H., W.C., and C.Y. assisted with sampling and laboratory analyses. All authors have given approval to the final version of the manuscript.

Funding

This research was funded by Chongqing Natural Science Foundation Surface Project, grant number cstc2019cyj-msxmX0788, and Scientific Research Fund of Chongqing Municipal Education Commission (KJQN201901342 and KJQN202001317).

Notes

The authors declare no competing financial interest.

■ ACKNOWLEDGMENTS

The authors express their gratitude to the reviewer and editor for their helpful comments to improve this manuscript.

■ REFERENCES

- (1) Fan, H.; Li, Q.; Li, K.; Hou, C.; Zhang, Q.; Li, Y.; Wang, H. Stretchable electrochromic fibers based on hierarchical porous structures with electrically conductive dual-pathways. *Sci. China Mater.* **2020**, *63*, 2582–2589.
- (2) Zhang, X. A.; Yu, S.; Xu, B.; Li, M.; Peng, Z.; Wang, Y.; Deng, S.; Wu, X.; Wu, Z.; Ouyang, M.; et al. Dynamic gating of infrared radiation in a textile. *Science* **2019**, *363*, 619–623.
- (3) Papa, I.; Russo, P.; Astarita, A.; Viscusi, A.; Perna, A. S.; Carrino, L.; Lopresto, V. Impact behaviour of a novel composite structure made of a polymer reinforced composite with a 3D printed metallic coating. *Compos. Struct.* **2020**, *245*, 112346.
- (4) Bayaniahangar, R.; Ahangar, S. B.; Zhang, Z.; Lee, B. P.; Pearce, J. M. 3-D printed soft magnetic helical coil actuators of iron oxide embedded polydimethylsiloxane. *Sens. Actuators, B* **2021**, *326*, 128781.

- (5) Zhou, J.; Xu, X. Z.; Xin, Y. Y.; Lubineau, G. Coaxial Thermoplastic Elastomer-Wrapped Carbon Nanotube Fibers for Deformable and Wearable Strain Sensors. *Adv. Funct. Mater.* **2018**, *28*, 1705591.
- (6) Lima, R. M. A. P.; Alcaraz-Espinoza, J. J.; da Silva, F. A. G., Jr.; de Oliveira, H. P. Multifunctional Wearable Electronic Textiles Using Cotton Fibers with Polypyrrole and Carbon Nanotubes. *ACS Appl. Mater. Interfaces* **2018**, *10*, 13783–13795.
- (7) Park, M.; Im, J.; Shin, M.; Min, Y.; Park, J.; Cho, H.; Park, S.; Shim, M.-B.; Jeon, S.; Chung, D.-Y.; et al. Highly stretchable electric circuits from a composite material of silver nanoparticles and elastomeric fibres. *Nat. Nanotechnol.* **2012**, *7*, 803–809.
- (8) Liu, Z. F.; Fang, S.; Moura, F. A.; Ding, J. N.; Jiang, N.; Di, J.; Zhang, M.; Lepró, X.; Galvão, D. S.; Haines, C. S.; Yuan, N. Y.; Yin, S. G.; Lee, D. W.; Wang, R.; Wang, H. Y.; Lv, W.; Dong, C.; Zhang, R. C.; Chen, M. J.; Yin, Q.; Chong, Y. T.; Zhang, R.; Wang, X.; Lima, M. D.; Ovalle-Robles, R.; Qian, D.; Lu, H.; Baughman, R. H. Hierarchically buckled sheath-core fibers for superelastic electronics, sensors, and muscles. *Science* **2015**, *349*, 400–404.
- (9) Ma, T.; Gao, H.-L.; Cong, H.-P.; Yao, H.-B.; Wu, L.; Yu, Z.-Y.; Chen, S.-M.; Yu, S.-H. A Bioinspired Interface Design for Improving the Strength and Electrical Conductivity of Graphene-Based Fibers. *Adv. Mater.* **2018**, *30*, 1706435.
- (10) Zhou, Y.; Fang, J.; Wang, H. X.; Zhou, H.; Yan, G. L.; Zhao, Y.; Dai, L. M.; Lin, T. Multicolor Electrochromic Fibers with Helix-Patterned Electrodes. *Adv. Electron. Mater.* **2018**, *4*, 1800104.
- (11) Ren, Y.; Sun, X. Y.; Liu, J. Advances in Liquid Metal-Enabled Flexible and Wearable Sensors. *Micromachines* **2020**, *11*, 200.
- (12) Chen, G.; Wang, H.; Guo, R.; Duan, M.; Zhang, Y.; Liu, J. Superelastic EGaIn Composite Fibers Sustaining 500% Tensile Strain with Superior Electrical Conductivity for Wearable Electronics. *ACS Appl. Mater. Interfaces* **2020**, *12*, 6112–6118.
- (13) Zhao, Z.-N.; Lin, J.; Zhang, J.; Yu, Y.; Yuan, B.; Fan, C.-C.; Wang, L.; Liu, J. Liquid Metal Enabled Flexible Electronic System for Eye Movement Tracking. *IEEE Sensor. J.* **2018**, *18*, 2592–2598.
- (14) Liang, S.; Wang, C.; Li, F.; Song, G. Supported Cu/W/Mo/Ni-Liquid Metal Catalyst with Core-Shell Structure for Photocatalytic Degradation. *Catalysts* **2021**, *11*, 1419.
- (15) Ren, Y.; Wang, X.; Liu, J. Fabrication of High-Resolution Flexible Circuits and Sensors Based on Liquid Metal Inks by Spraying and Wiping Processing. *IEEE Trans. Biomed. Circuits Syst.* **2019**, *13*, 1545–1551.
- (16) Malakooti, M. H.; Bockstaller, M. R.; Matyjaszewski, K.; Majidi, C. Liquid metal nanocomposites. *Nanoscale Adv.* **2020**, *2*, 2668–2677.
- (17) Tang, J.; Lambie, S.; Meftahi, N.; Christofferson, A. J.; Yang, J.; Ghasemian, M. B.; Han, J.; Allieux, F.-M.; Rahim, M. A.; Mayyas, M.; et al. Unique surface patterns emerging during solidification of liquid metal alloys. *Nat. Commun.* **2021**, *16*, 431–439.
- (18) Kalantar-Zadeh, K.; Rahim, M. A.; Tang, J. Low Melting Temperature Liquid Metals and Their Impacts on Physical Chemistry. *Acc. Mater. Res.* **2021**, *2*, 577–580.
- (19) He, J.; Liang, S.; Li, F.; Yang, Q.; Huang, M.; He, Y.; Fan, X.; Wu, M. Recent Development in Liquid Metal Materials. *Chemistryopen* **2021**, *10*, 360–372.
- (20) Lu, H.; Yun, G.; Cole, T.; Ouyang, Y.; Ren, H.; Shu, J.; Zhang, Y.; Zhang, S.; Dickey, M. D.; Li, W.; Tang, S.-Y. Reversible Underwater Adhesion for Soft Robotic Feet by Leveraging Electrochemically Tunable Liquid Metal Interfaces. *ACS Appl. Mater. Interfaces* **2021**, *13*, 37904–37914.
- (21) Allieux, F.-M.; Han, J.; Tang, J.; Merhebi, S.; Cai, S.; Tang, J.; Abbasi, R.; Centurion, F.; Mousavi, M.; Zhang, C.; Xie, W.; Mayyas, M.; Rahim, M. A.; Ghasemian, M. B.; Kalantar-Zadeh, K. Nanotip Formation from Liquid Metals for Soft Electronic Junctions. *ACS Appl. Mater. Interfaces* **2021**, *13*, 43247–43257.
- (22) Liao, M.; Liao, H.; Ye, J.; Wan, P.; Zhang, L. Polyvinyl Alcohol-Stabilized Liquid Metal Hydrogel for Wearable Transient Epidermal Sensors. *ACS Appl. Mater. Interfaces* **2019**, *11*, 47358–47364.
- (23) Zhang, R.; Ye, Z.; Gao, M.; Gao, C.; Zhang, X.; Li, L.; Gui, L. Liquid metal electrode-enabled flexible microdroplet sensor. *Lab Chip* **2020**, *20*, 496–504.
- (24) Guo, R.; Wang, H.; Chen, G.; Yuan, B.; Zhang, Y.; Liu, J. Smart semiliquid metal fibers with designed mechanical properties for room temperature stimulus response and liquid welding. *Appl. Mater. Today* **2020**, *20*, 100738.
- (25) Liu, H.; Xin, Y.; Lou, Y.; Peng, Y.; Wei, L.; Zhang, J. Liquid metal gradient fibers with reversible thermal programmability. *Mater. Horiz.* **2020**, *7*, 2141–2149.
- (26) Dong, C.; Leber, A.; Das Gupta, T.; Chandran, R.; Volpi, M.; Qu, Y.; Nguyen-Dang, T.; Bartolomei, N.; Yan, W.; Sorin, F. High-efficiency super-elastic liquid metal based triboelectric fibers and textiles. *Nat. Commun.* **2020**, *11*, 3537–3546.
- (27) Schermer, R. T.; Villarruel, C. A.; Bucholtz, F.; McLaughlin, C. V. Reconfigurable liquid metal fiber-optic mirror for continuous, widely-tunable true-time-delay. *Opt. Express* **2013**, *21*, 2741–2747.
- (28) Yan, J.; Lu, Y.; Chen, G.; Yang, M.; Gu, Z. Advances in liquid metals for biomedical applications. *Chem. Soc. Rev.* **2018**, *47*, 2518–2533.
- (29) Xie, W.; Allieux, F.-M.; Namivandi-Zangeneh, R.; Ghasemian, M. B.; Han, J.; Rahim, M. A.; Tang, J.; Yang, J.; Mousavi, M.; Mayyas, M.; et al. Polydopamine Shell as a Ga³⁺ Reservoir for Triggering Gallium–Indium Phase Separation in Eutectic Gallium–Indium Nanoalloys. *ACS Nano* **2021**, *15*, 16839–16850.
- (30) Zhang, C.; Allieux, F.-M.; Rahim, M. A.; Han, J.; Tang, J.; Ghasemian, M. B.; Tang, S.-Y.; Mayyas, M.; Daeneke, T.; Le-Clech, P.; et al. Nucleation and Growth of Polyaniline Nanofibers onto Liquid Metal Nanoparticles. *Chem. Mater.* **2020**, *32*, 4808–4819.
- (31) Lai, Y.-C.; Lu, H.-W.; Wu, H.-M.; Zhang, D.; Yang, J.; Ma, J.; Shamsi, M.; Vallem, V.; Dickey, M. D. Elastic Multifunctional Liquid-Metal Fibers for Harvesting Mechanical and Electromagnetic Energy and as Self-Powered Sensors. *Adv. Energy Mater.* **2021**, *11*, 2100411.
- (32) Zhang, M.; Wang, X.; Huang, Z.; Rao, W. Liquid Metal Based Flexible and Implantable Biosensors. *Biosensors* **2020**, *10*, 170.
- (33) Baharfar, M.; Mayyas, M.; Rahbar, M.; Allieux, F.-M.; Tang, J.; Wang, Y.; Cao, Z.; Centurion, F.; Jalili, R.; Liu, G.; Kalantar-Zadeh, K. Exploring Interfacial Graphene Oxide Reduction by Liquid Metals: Application in Selective Biosensing. *ACS Nano* **2021**, *15*, 19661–19671.
- (34) Wu, Y.-h.; Zhen, R.-m.; Liu, H.-z.; Liu, S.-q.; Deng, Z.-f.; Wang, P.-p.; Chen, S.; Liu, L. Liquid metal fiber composed of a tubular channel as a high-performance strain sensor. *J. Mater. Chem. C* **2017**, *5*, 12483–12491.
- (35) Cooper, C. B.; Arutselvan, K.; Liu, Y.; Armstrong, D.; Lin, Y. L.; Khan, M. R.; Genzer, J.; Dickey, M. D. Stretchable Capacitive Sensors of Torsion, Strain, and Touch Using Double Helix Liquid Metal Fibers. *Adv. Funct. Mater.* **2017**, *20*, 1605630.
- (36) Zheng, L.; Zhu, M.; Wu, B.; Li, Z.; Sun, S.; Wu, P. Conductance-stable liquid metal sheath-core microfibers for stretchy smart fabrics and self-powered sensing. *Sci. Adv.* **2021**, *7*, No. eabg4041.